Eur. Phys. J. D **23**, 237–255 (2003)
DOI: 10.1140/epjd/e2003-00098-4

THE EUROPEAN PHYSICAL JOURNAL D

Resonant coupling in the van der Waals interaction between an excited alkali atom and a dielectric surface: an experimental study via stepwise selective reflection spectroscopy

H. Failache[a], S. Saltiel[b], M. Fichet, D. Bloch[c], and M. Ducloy

Laboratoire de Physique des Lasers, UMR 7538 du CNRS, Institut Galilée, Université Paris-13, 99 avenue J.-B. Clément, 93430 Villetaneuse, France

Received 16 January 2003 / Received in final form 25 March 2003
Published online 5 May 2003

Abstract. We present a detailed experimental study of the evaluation of the van der Waals (vW) atom-surface interaction for high-lying excited states of alkali-metal atoms (Cs and Rb), notably when they couple resonantly with a surface-polariton mode of the neighbouring dielectric surface. This report extends our initial observation [Phys. Rev. Lett. **83**, 5467 (1999)] of a vW repulsion between $Cs(6D_{3/2})$ and a sapphire surface. The experiment is based upon FM selective reflection spectroscopy, on a transition reaching a high-lying state from a resonance level, that has been thermally pumped by an initial one-photon step. Along with a strong vW repulsion fitted with a blue lineshift, -160 ± 25 kHz μm^3 for $Cs(6D_{3/2})$ in front of a sapphire surface (with a perpendicular c-axis), we demonstrate a weaker vW repulsion (-32 ± 5 kHz μm^3) for $Cs(6D_{3/2})$ in front of a YAG surface, as due to a similar resonant coupling at 12 μm between a virtual atomic emission ($6D_{3/2}$–$7P_{1/2}$) and the surface polariton modes. A resonant behaviour of $Rb(6D_{5/2})$ in front of a sapphire surface exists also because of analogous decay channels in the 12 μm range. Finally, one demonstrates that fused silica, nonresonant for a virtual transition in the 12 μm range and hence weakly attracting for $Cs(6D_{3/2})$, exhibits a resonant behaviour for $Cs(9S_{1/2})$ as due to its surface polariton resonance in the 8–9 μm range. The limiting factors that affect both the accuracy of the theoretical prediction, and that of the fitting method applied to the experimental data, are discussed in the conclusion.

PACS. 42.50.Xa Optical tests of quantum theory – 34.50.Dy Interactions of atoms and molecules with surfaces; photon and electron emission; neutralization of ions – 42.50.Ct Quantum description of interaction of light and matter; related experiments – 32.70.Jz Line shapes, widths, and shifts – 78.20.Ci Optical constants (including refractive index, complex dielectric constant, absorption, reflection and transmission coefficients, emissivity)

1 Introduction

The long-range forces between an atom and a surface [1] have a fundamental importance which affects numerous domains of physical sciences, and the control of these forces could open new avenues for various engineering purposes. Because the coupling between a (fluctuating) dipole and its electrostatic image is attractive, the nonretarded van der Waals (vW) surface interaction between an atom and a perfect reflector is often thought to be universally attractive. Actually, for an atom in front of a real surface, like a dielectric medium, one cannot ignore the dispersive properties of the surface in the frequency range of the quantized atom fluctuations. Situations can occur in which the virtual emission of an atom resonantly couples with the electromagnetic (e.m.) modes of the surface [2–4], *e.g.* a surface polariton mode. In this case, the atom-surface interaction is magnified, while the delay between the original atomic fluctuations and the image induced in the surface is susceptible to turn the attractive behaviour into a repulsion.

We have previously reported [5] on the first observation of this resonant atom-surface coupling, and on the spectroscopic evidence of a repulsive atom-surface potential. In this paper, we elaborate our experimental results. They are based on an optical method of selective reflection (SR) spectroscopy between excited states, that probes

[a] *Now at* IFFI, Universidad de la Republica, Montevideo, Uruguay.
[b] *Permanent address*: Dept of Physics, Sofia University, Bulgaria.
[c] e-mail: bloch@galilee.univ-paris13.fr

the vapour in the vicinity of an interface within a typical range $\lambda/2\pi$, with λ the optical wavelength of the probe. Through an adequate first step pumping, we have extended to excited states our previously demonstrated ability [6–10] to measure the van der Waals interaction from a transition starting from a thermally populated ground state.

The main study [5,11] has dealt with $Cs(6D_{3/2})$ because of a virtual emission at 12.15 μm (towards $7P_{1/2}$), that falls within the resonance of polariton modes of sapphire, as estimated [3] from older literature [12]. For purposes of comparison, we have also tested various types of sapphire windows, differing notably by the orientation of their c-axis, and have studied the vW interaction exerted on $Cs(6D_{3/2})$ by other materials, like a fused silica window and a YAG window. An extension [11] of this study includes some attempts to evaluate the vW surface interaction exerted on Rb(6D), as motivated by a special coincidence: the $6D_{3/2}$ and $6D_{5/2}$ levels of Rb are respectively connected to $7P_{1/2}$ and $7P_{3/2}$ by virtual emission falling into the sapphire resonance range at 12 μm. In another extension, we have investigated the $Cs(9S_{1/2})$ level, because of a virtual emission in the 8–9 μm range for which a fused silica surface could exhibit a resonant coupling, and a sapphire surface a nonresonant one.

The discussion is organized as follows. In a first part (Sect. 2) we recall the main theoretical elements required to predict the vW interaction exerted onto an excited atom by a surface in the case of resonant coupling. This is illustrated with experimental data from the literature that are relevant to predict the vW interaction. The next section (Sect. 3) is devoted to the experimental set-up of SR spectroscopy at an interface and includes the extension to transitions between excited states. In Section 4, which is central to this report, we present the interpretation of the various experimental data for $Cs(6D_{3/2})$ as obtained through an elaborate fitting method. In Section 5, we report on the results obtained for Rb(6D), while Section 6 deals with the Cs(9S) results.

2 Theoretical predictions for the strength of the surface vW interaction

2.1 vW interaction between an atom and a reflecting surface

It is well-known [13] that when an atom lies in front of a perfect reflector, its energy structure, as defined in vacuum, is modified as due to the e.m. coupling between the atomic quantum fluctuations and the fluctuations induced in the reflector (in an alternate point of view, the vacuum fluctuations are modified because of the boundary conditions imposed by the perfect reflector). The long-range interaction is essentially defined by its insensitivity to the atomic details of the dense surface. It can be described by an effective Hamiltonian:

$$H = -\frac{1}{64\pi\varepsilon_0 z^3}\left(\mathbf{D}^2 + D_z^2\right). \tag{1}$$

In (1), $\mathbf{D}$ is the atomic dipole operator, D_z its component along the normal Oz to the surface, and z the distance between the surface and the atom. Equation (1) is restricted to the *nonretarded limit*, which usually defines the range of the surface vW interaction. This description implies to neglect the propagation effects, that attenuates the z^{-3} interaction towards a z^{-4} attraction (*i.e.* the relativistic Casimir-Polder limit [15]) for an atom in its ground state, or that oscillates with contributions in $z^{-1}\cos(kz)$, or $z^{-2}\sin(kz)$ in the case of an excited state [14,16] (with k the spatial period associated to the wavelength of the spontaneous emission from the excited state). More precisely, the nonretarded approximation is verified as long as $z \ll \lambda_\alpha$, with λ_α standing for the wavelength of the generic virtual dipole transitions coupling the considered atomic level to other levels. Within this approximation, and assuming here for simplicity that the atom is isotropic (*i.e.* the operator $(\mathbf{D}^2 + D_z^2)$ is equivalent to $4D^2/3$), the interaction of an atom in the $|i\rangle$ level with a perfect reflector corresponds to an energy modified by ΔE_i:

$$\Delta E_i = -\frac{4}{3}\frac{1}{64\pi\varepsilon_0 z^3}\left\langle i\left|D^2\right|i\right\rangle \tag{2a}$$

$$= -\frac{1}{48\pi\varepsilon_0 z^3}\sum_j \langle i\,|D|\,j\rangle\,\langle j\,|D|\,i\rangle \tag{2b}$$

$$= -C_3/z^3. \tag{2c}$$

The remarkable point shown in (2b) is that the *strength* of the vW interaction depends on an explicit sum over all virtual dipole transitions from level $|i\rangle$. The knowledge of these purely atomic couplings is essential for the determination of the vW interaction. In most cases, because the dipole moment $\langle i|D|j\rangle$ is related to the transition probability by a factor involving the third power of the wavelength $(\lambda_{ij})^3$, (λ_{ij} the wavelength of the $i \to j$ transition), the dominant contribution originates in atomic couplings with neighbouring states, for which the relative probability of a real transition is weak. This can be illustrated with the example, discussed in more detail below, of $Cs(6D_{3/2})$ for which the transition $6D_{3/2} \to 7P_{1/2}$ approximately accounts for only 5×10^{-3} of the 50 ns spontaneous emission lifetime of level $6D_{3/2}$, but provides about 20% of the vW shift in front of a perfect reflector.

2.2 Interaction with a dielectric surface

If the ideal reflector is replaced by a dielectric surface, the z^{-3} vW surface interaction is modified by a "dielectric image" factor. While in electrostatics, the image factor would be simply given by $S = (\varepsilon - 1)/(\varepsilon + 1)$, here, the vW interaction originates in quantum fluctuations, and the dispersive properties of the dielectric medium cannot be ignored. Hence, a frequency-dependent dielectric image coefficient $r(\omega_{ij})$ has to be applied to each contribution associated to a virtual dipole coupling [3]:

$$\Delta E_i = -\frac{1}{48\pi\varepsilon_0 z^3}\sum_j r(\omega_{ij})\langle i|D|j\rangle\langle j|D|i\rangle \tag{3}$$

with ω_{ij} the frequency associated with the virtual coupling $|i\rangle \rightarrow |j\rangle$.

As long as the $|i\rangle$ level is the ground state, ω_{ij} is simply the frequency for a virtual absorption (by convention we take this frequency to be positive), and the corresponding image coefficient $r(\omega_{ij})$ satisfies $0 \leq r(\omega_{ij}) \leq 1$, with $r(\omega_{ij})$ given by [2,3,17]:

$$r(\omega_{ij} > 0) = \frac{2}{\pi} \int_0^\infty S(\mathrm{i}u) \frac{\omega_{ij}}{\omega_{ij}^2 + u^2} \mathrm{d}u \qquad (4)$$

in which S is the surface response:

$$S(\omega) = \frac{\varepsilon(\omega) - 1}{\varepsilon(\omega) + 1}. \qquad (5)$$

In (4), $S(\mathrm{i}u)$ and $\varepsilon(\mathrm{i}u)$ are respectively the surface response and the permittivity taken at the imaginary frequency $\mathrm{i}u$, as analytically extended in the complex plane from the dispersive properties of the dielectric constants of the material at the interface. Due to this analytical extension and causality, one predicts the monotonous behaviour of $\varepsilon(\mathrm{i}u)$ and $S(\mathrm{i}u)$, that imposes $0 \leq r(\omega_{ij}) \leq 1$.

For an excited state $|i\rangle$, one has to distinguish [2,3] between virtual absorption and virtual emission. For contributions associated with a virtual absorption (*i.e.* $E_j > E_i$), the expression for $r(\omega_{ij})$ remains essentially similar to the case when $|i\rangle$ is the ground state (*i.e.* Eq. (4) applies). For contributions originating in a virtual emission ($\omega_{ij} < 0$ according to our convention), $r(\omega_{ij})$ includes an additional contribution, that offers possibilities of a resonance. Indeed, one has:

$$r(\omega_{ij} < 0) = -\frac{2}{\pi} \int_0^\infty S(\mathrm{i}u) \frac{|\omega_{ij}|}{\omega_{ij}^2 + u^2} \mathrm{d}u + 2\mathrm{Re}S(|\omega_{ij}|). \qquad (6)$$

One notices that the second term in the r.h.s. of equation (6) can drastically modify the amplitude, and sign, of $r(\omega_{ij})$. This notably happens when the virtual dipole emission at ω_{ij} falls in an absorption band of the dense medium. In particular, the surface response $\mathrm{Re}S(\omega)$ can take large values at some specific frequencies, related to the poles of the surface polariton modes given by the poles of $S(\omega)$. The poles are usually defined by a complex frequency for which $\mathrm{Re}S(\omega)$ would diverge. On the real frequency axis, this simply leads to a resonant behaviour in the surface response. The atom interaction with the dielectric surface can hence be seen as driven by a resonant coupling between a virtual atomic emission, and a virtual absorption in a surface mode.

2.3 Evaluation of the surface response for several materials

Generally, an accurate evaluation of $r(\omega_{ij})$ is a difficult task. First, an extensive spectral evaluation of $\varepsilon(\omega)$ appears to be required as equation (4) includes a frequency integration over the dielectric spectral response (note that in (4), one could introduce $\varepsilon(\omega)$ instead of $\varepsilon(\mathrm{i}u)$ [3], but one is left anyhow with the need of a frequency integration over the whole spectrum). This is actually not the most critical point to evaluate the resonant contribution. A more sensible point is that $\varepsilon(\omega_{ij})$ is not measured directly, but rather extrapolated from various types of measurements, most often of the reflectance-type (this is related with the fact that the medium is opaque in the region of interest). Another difficulty is related with the variations from sample to sample as due to impurities, crystal growth, sample temperature, or to surface defects (possibly critical for reflective measurements). These points will be discussed at length in a critical evaluation of $r(\omega_{ij})$ [18], based on the published optical data for several types of windows.

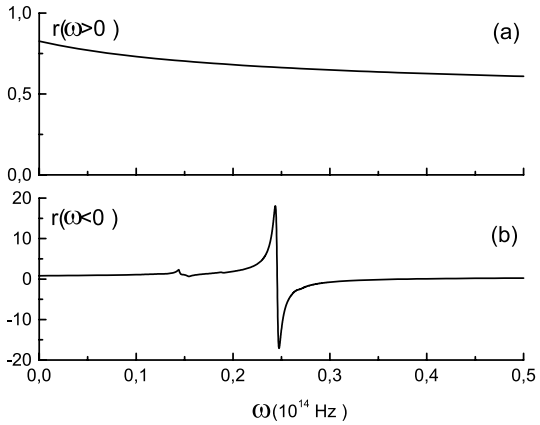

Fig. 1. Dielectric image coefficient for a sapphire interface (optical axis normal to the interface, $c\perp$) as a function of the virtual transition frequency; (a) absorption $\omega > 0$, (b) emission $\omega < 0$.

We evaluate the sapphire surface response on a large spectral range, including both cases of virtual emission and virtual absorption of the atom. The data are obtained from an analytic evaluation extrapolated from [19], using the Drude-Lorentz model. For a virtual coupling in absorption, $r(\omega_{ij} > 0)$ smoothly decreases (Fig. 1a) from values on the order of 0.83 for the far infrared to 0.47 in the visible. For an atomic coupling in *emission*, the sapphire surface response $r(\omega_{ij} < 0)$ is essentially characterized by a main peak around 12 μm (dispersion-like lineshape, quality factor $\cong 10^2$, peak value ≤ 20), and a secondary one around 20 μm (Fig. 1b). These surface resonances can be seen as reminiscent of the respective 15 μm and 20–24 μm absorption bands of the bulk sapphire. An extra-difficulty is associated with the natural birefringence of sapphire. It induces a removal of degeneracy in the surface polariton resonances [3]. The consequences for the atom-surface interaction have been studied recently [4]. Here, we simply recall that sapphire is a uniaxial material and that the usual cylindrical symmetry of the vW interaction is not broken for a c-axis oriented normally to the surface ($c\perp$). Hence, the expression for $r(\omega_{ij})$ [Eqs. (4–6)] is valid provided an effective permittivity $\bar{\varepsilon} = \sqrt{\varepsilon_o \varepsilon_e}$ is considered (ε_o and ε_e are the permittivities respectively associated with the ordinary and extraordinary indices, the square root being the determination continuously

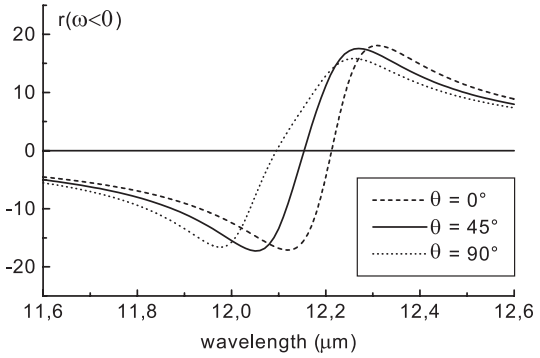

Fig. 2. Tuning of the sapphire polariton resonance through c-axis orientation (θ is the angle between the c-axis and the normal to the interface).

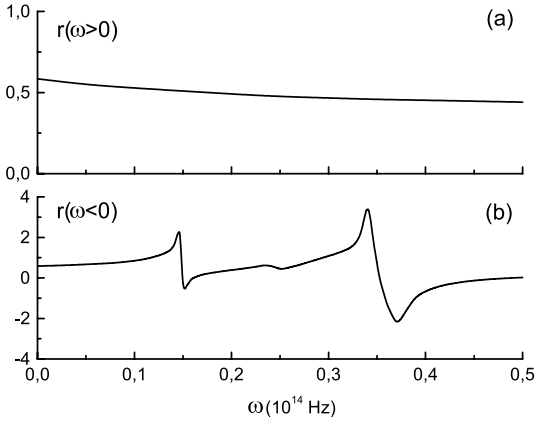

Fig. 3. Dielectric image coefficient for a fused silica (SiO_2) interface as a function of the virtual frequency; (a) absorption $\omega > 0$, (b) emission $\omega < 0$.

extended from the frequency range where ε_o and ε_e take real values) [3]. For a ($c\perp$) window, one has predicted a polariton resonance approximately centred at 12.2 μm (Fig. 1b). From [4], and neglecting the break of the cylindrical symmetry (*e.g.* for an atomic state with a sufficient symmetry, like an s-state, or a p-state), one would find for a c-axis parallel to the window ($c\|$), a resonance centre shifted to 12.1 μm (*i.e.* a blue polariton shift of 8 cm^{-1}). For an arbitrary c-axis orientation, the resonant behaviour evolves smoothly between the two typical situations mentioned above (Fig. 2).

For a fused silica window (Fig. 3) the predicted resonances (*i.e.* for $\omega_{ij} < 0$) have to be extrapolated from data that appear to be even more sensitive to the considered sample than for a crystalline window [20]. The surface resonances essentially include two isolated dispersion-like resonances, one centred in the 8–9 μm region, and the other one in the 20 μm region, with respective amplitudes on the order of +3.38, −2.15 and +2.27, −0.53. A third minor resonance (whose effects could be however relatively dramatic in our experiments) is predicted around 12 μm.

We have used also windows made of YAG ($Y_3Al_5O_{12}$), a material of interest because its chemical resistance to a high temperature alkali vapour is comparable with the one

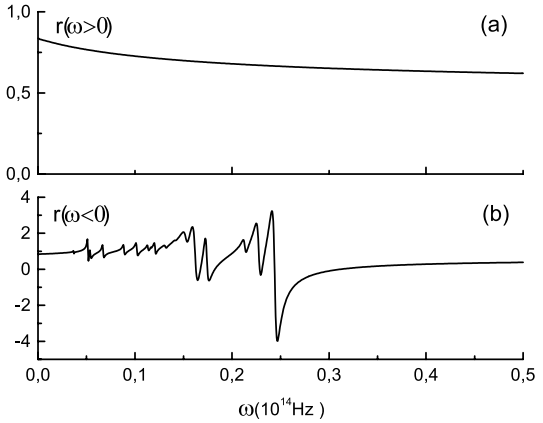

Fig. 4. Dielectric image coefficient for a YAG ($Y_3Al_5O_{12}$) interface as a function of the virtual frequency; (a) absorption $\omega > 0$, (b) emission $\omega < 0$.

of sapphire (*i.e.* much higher than the one of a fused silica). Surface resonances for YAG [18] are located in the 10–60 μm range (Fig. 4). They are more numerous than those of sapphire or glass, reflecting the numerous phonon resonances of the bulk material [21]. In return, these surface resonances have a relatively low amplitude. It is accompanied by a partial overlap of the resonances, so that the non resonant contribution in equation (6) (*i.e.* the first term in the r.h.s.) is non-negligible. This makes the lineshapes for $r(\omega_{ij} < 0)$ no longer resembling an antisymmetric dispersion lineshape.

2.4 vW coupling for the relevant excited states

Alkali atoms in the free-space have a well-known structure, and the surface vW interaction exerted by a perfect reflector can be evaluated straightforwardly (most often through theoretical estimates, rather than from direct experimental measurements, of the dipolar transition moment). As a rule, the higher the atomic excitation, the higher is the surface interaction, with an asymptotic behaviour [13] growing like $(n^*)^4$ (with n^* the effective quantum number). In our case, we have performed SR spectroscopy on transitions between excited states of Cs and Rb, starting respectively from the resonance levels $6P_{1/2}$ and $5P_{3/2}$ levels. For these initial levels, the perfect reflector C_3 coefficient had been evaluated in previous works to $C_3 = 4.43$ kHz μm^3 for Cs and $C_3 = 4.59$ kHz μm^3 for Rb [11] ([22]). These values are to be considered as an upper limit for the interaction with any of the considered windows. Indeed, for these first resonance levels, the virtual couplings in emission (*i.e.* coupling towards the ground state) lie in the transparency region of the considered windows, implying $0 < r(\omega_v) < 1$ whatever is the involved virtual transitions. Conversely, for the upper states studied in the present work, whose "perfect reflector" values of the interaction strength are $C_3 = 25.3$ kHz μm^3 for Cs($6D_{3/2}$) level, $C_3 = 82.4$ kHz μm^3 for Rb($6D_{3/2}$) level and $C_3 = 81.2$ kHz μm^3 for Rb($6D_{5/2}$) level (see Tabs. 1–3 calculated using previous data in the literature [23,24]),

Table 1. The predicted vW shift for $Cs(6D_{3/2})$ in the vicinity of various interfaces, with the contribution of each relevant virtual transition. The sign (−) in the wavelength column is for emission coupling.

$Cs(6D_{3/2})$	λ (μm)	$\delta\nu$ vW perfect reflector kHz μm^3	$\delta\nu$ vW sapphire $c_\perp$ kHz μm^3	$\delta\nu$ vW YAG kHz μm^3	$\delta\nu$ vW fused silica kHz μm^3
$6P_{1/2}$	(−)0.87637	0.382	0.205	0.217	0.129
$6P_{3/2}$	(−)0.92110	0.093	0.05	0.053	0.031
$7P_{1/2}$	(−)12.147	6.756	−108.67	−26.91	3.323
$7P_{3/2}$	(−)15.571	1.377	2.237	0.796	0.470
$8P_{1/2}$	3.2040	0.505	0.286	0.297	0.205
$8P_{3/2}$	3.1213	0.060	0.034	0.035	0.024
$9P_{1/2}$	1.9803	0.045	0.024	0.025	0.017
$10P_{1/2}$	1.6287	0.011	0.006	0.006	0.004
$4F_{5/2}$	5.3083	15.28	9.172	9.374	6.593
$5F_{5/2}$	2.2812	0.339	0.185	0.195	0.134
$6F_{5/2}$	1.7419	0.177	0.094	0.01	0.068
$7F_{5/2}$	1.5245	0.096	0.05	0.054	0.037
$8F_{5/2}$	1.4104	0.057	0.03	0.032	0.022
$9F_{5/2}$	1.3416	0.037	0.019	0.020	0.014
$10F_{5/2}$	1.2964	0.025	0.013	0.014	0.01
$11F_{5/2}$	1.2649	0.018	0.009	0.01	0.007
$12F_{5/2}$	1.2419	0.014	0.007	0.007	0.005
Total		25.27	−96.25	−15.77	11.09

Table 2. Same as Table 1 for $Rb(6D_{5/2})$.

$Rb(6D_{5/2})$	λ (μm)	$\delta\nu$ vW perfect reflector kHz μm^3	$\delta\nu$ vW sapphire $c_\perp$ kHz μm^3	$\delta\nu$ vW YAG kHz μm^3	$\delta\nu$ vW fused silica kHz μm^3
$5P_{3/2}$	(−)0.63001	0.032	0.018	0.018	0.011
$6P_{3/2}$	(−)2.0422	0.082	0.039	0.043	0.025
$7P_{3/2}$	(−)12.206	24.671	−58.354	−89.594	12.58
$8P_{3/2}$	8.5880	7.161	4.557	4.598	3.294
$9P_{3/2}$	4.3844	0.442	0.259	0.266	0.185
$10P_{3/2}$	3.3650	0.117	0.067	0.069	0.048
$11P_{3/2}$	2.9162	0.055	0.031	0.032	0.022
$12P_{3/2}$	2.6684	0.029	0.016	0.017	0.011
$4F_{5/2-7/2}$	(−)5.2703	1.746	0.532	0.729	0.209
$5F_{5/2-7/2}$	17.002	44.037	30.403	30.306	22.018
$6F_{5/2-7/2}$	5.1590	1.575	0.942	0.964	0.677
$7F_{5/2-7/2}$	3.6736	0.613	0.353	0.364	0.251
$8F_{5/2-7/2}$	3.0488	0.285	0.160	0.167	0.114
$9F_{5/2-7/2}$	2.7458	0.161	0.089	0.093	0.064
$10F_{5/2-7/2}$	2.5637	0.101	0.056	0.058	0.040
$11F_{5/2-7/2}$	2.4439	0.068	0.038	0.039	0.027
$12F_{5/2-7/2}$	2.3600	0.048	0.027	0.028	0.019
Total		81.22	−20.77	−51.80	39.59

a large variety of *emission* couplings can exist. Hence, it becomes possible to explore experimentally the resonances of various materials. In a previous analysis [3], we had shown that the contribution of the $6D_{3/2}$–$7P_{1/2}$ emission for Cs, located in the IR range at 12.15 μm, and that accounts for ∼25% of the vW interaction for a perfect reflector, falls in the region of strong sapphire surface resonance (conversely, the $6D_{5/2}$ is only coupled to $7P_{3/2}$ at 14.6 μm, not yielding resonances). Tables 1–3 show an up-to-date of these calculations extended to the relevant levels of interest for Cs and Rb [25]. The values used for $r(\omega_{ij})$ in Table 1 are estimated from the same data, whose accuracy was discussed above (Sect. 2.3), as presented in Figures 1, 3 and 4. Hence large uncertainties are expected in the theoretical evaluations for a given system "excited atom/dielectric surface". In particular, for $Cs(6D_{3/2})$,

Table 3. Same as Table 1 for $Rb(6D_{3/2})$.

$Rb(6D_{3/2})$	λ (μm)	$\delta\nu$ vW perfect reflector kHz μm^3	$\delta\nu$ vW sapphire $c_\perp$ kHz μm^3	$\delta\nu$ vW YAG kHz μm^3	$\delta\nu$ vW fused silica kHz μm^3
$5P_{1/2}$	$(-)0.6208$	0.025	0.014	0.014	0.009
$6P_{1/2}$	$(-)2.0113$	0.031	0.015	0.016	0.009
$6P_{3/2}$	$(-)2.0431$	0.014	0.006	0.007	0.004
$7P_{1/2}$	$(-)11.736$	18.273	-109.054	-31.585	8.612
$7P_{3/2}$	$(-)12.240$	4.147	39.296	-11.532	2.174
$8P_{3/2}$	8.5714	1.192	0.758	0.765	0.546
$8P_{1/2}$	8.7122	6.643	4.235	4.271	3.019
$9P_{3/2}$	4.3801	0.073	0.043	0.044	0.031
$9P_{1/2}$	4.4018	0.371	0.218	0.224	0.156
$10P_{3/2}$	3.3624	0.019	0.011	0.012	0.008
$10P_{1/2}$	3.3707	0.094	0.053	0.055	0.038
$11P_{1/2-3/2}$	2.9143	0.049	0.028	0.029	0.020
$12P_{1/2-3/2}$	2.6667	0.026	0.014	0.015	0.010
$4F_{5/2}$	$(-)5.2766$	1.752	0.533	0.731	0.203
$5F_{5/2}$	16.937	46.644	32.189	32.091	23.196
$6F_{5/2}$	5.1530	1.681	1.006	1.029	0.724
$7F_{5/2}$	3.6306	0.634	0.364	0.377	0.261
$8F_{5/2}$	3.0647	0.310	0.175	0.182	0.125
$9F_{5/2}$	2.7441	0.172	0.096	0.100	0.069
$10F_{5/2}$	2.5622	0.108	0.060	0.062	0.043
$11F_{5/2}$	2.4426	0.073	0.040	0.042	0.029
$12F_{5/2}$	2.3587	0.052	0.028	0.030	0.020
Total		82.38	-29.87	-3.02	39.31

Table 4. Same as Table 1 for $Cs(9S_{1/2})$.

$Cs(9S_{1/2})$	λ (μm)	$\delta\nu$ vW perfect reflector (KHz μm^3)	$\delta\nu$ vW sapphire $c_\perp$ (KHz μm^3)	$\delta\nu$ vW fused silica (KHz μm^3)
$6P_{1/2}$	$(-)0.6356$	0.009	0.005	0.003
$6P_{3/2}$	$(-)0.6588$	0.020	0.011	0.007
$7P_{1/2}$	$(-)1.9436$	0.131	0.063	0.04
$7P_{3/2}$	$(-)2.014$	0.293	0.140	0.089
$8P_{1/2}$	$(-)8.323$	9.402	-0.871	-12.25
$8P_{3/2}$	$(-)8.937$	23.281	-6.044	62.60
$9P_{1/2}$	13.762	33.555	22.609	16.28
$9P_{3/2}$	12.965	56.106	37.540	27.099
$10P_{1/2}$	5.505	0.455	0.274	0.198
$10P_{3/2}$	5.427	0.872	0.525	0.378
$11P_{1/2}$	4.011	0.080	0.047	0.033
$11P_{3/2}$	3.983	0.157	0.091	0.065
$12P_{1/2}$	3.398	0.022	0.012	0.009
$12P_{3/2}$	3.385	0.043	0.025	0.018
Total		124.43	54.43	94.57

the overall vW interaction appears to be strongly dependent of the exact values of $r(\omega_{ij})$ for YAG on the 12.15 μm transition, while for fused silica, a possible modified value of the dielectric coefficient at 12.15 μm would induce only marginal changes. One also sees in Tables 2 and 3 that Rb(6D) is similarly coupled to the 7P level in the 12 μm range; this coincidence in the "low n Rydberg states" of alkali now includes $6D_{5/2}$ as well as $6D_{3/2}$, with respective couplings at 12.21 μm, and at 11.74 μm and 12.24 μm. An interesting point is that it may provide a sensitive way to test the sapphire surface resonances. For Cs ($9S_{1/2}$), as shown in Table 4, there is a strong emission coupling in the 9S–8P emission at 8.323 μm and 8.937 μm, that falls close to the expected surface resonances of fused silica, but far

from the sapphire or YAG surface resonances. Note that for most of those high-lying states studied here, only a single virtual transition determines the resonant coupling between the atom and the surface. This contrasts with the general situation encountered with highly excited states, such as Rydberg levels [13,14], when several emission couplings may compete as due to multiple resonances of the surface.

3 Description of the experiments

3.1 Principle of the experiments: selective reflection spectroscopy between excited states

Among the few experimental methods [14,26] that permits the observation of the atom-surface interaction, SR spectroscopy is particularly well-suited to the observation of interaction of a surface with short-lived atomic levels ([6] and references therein), owing to its combination of optical excitation and detection. SR spectroscopy essentially consists of monitoring the resonant change of reflectivity coefficient at the interface between the surface of interest, and the atomic vapour. Within the standard assumption of an optically dilute medium (*i.e.* when the propagation on a wavelength scale of the incident beam is not sensitively affected by the resonant interaction), the SR signal can be viewed as the homodyne beat between the nonresonant contribution of the field $E_{\rm NR}$ reflected at the interface, and the field $E_{\rm vap}$ that the vapour radiates as due to the oscillating dipole induced by the incident field in the direction of the reflected field. Assuming for sake of simplicity a normal incidence, this resonant radiated field is given by:

$$E_{\rm vap} = \frac{1}{2{\rm i}\varepsilon_0 k}\int_0^{+\infty} \exp(2{\rm i}kz)p(z){\rm d}z \qquad (7)$$

with k the spatial period of the incident wave, and $p(z)$ the amplitude of the oscillating dipole induced at z in the vapour by the resonant incident field. For a dilute vapour, one has $E_{\rm vap} \ll E_{\rm NR}$, and the measured SR signal given by $2{\rm Re}(E_{\rm NR}^* E_{\rm vap})$, is simply proportional to $2{\rm Re}(E_{\rm vap})$ (conventionally assuming that $E_{\rm NR}$ is real at the interface). In (7), the $\exp(2{\rm i}kz)$ factor is responsible for the finite coherence length of the radiative process leading to the build-up of $E_{\rm vap}$. As, far from the surface, the amplitude of the induced dipole tends to be independent of z, SR spectroscopy is particularly sensitive to inhomogeneities induced in the vicinity of the surface (within one – reduced – optical wavelength $\lambda/2\pi$), and hence to the atom-surface interaction.

Although the SR technique lies on a simple principle, the evaluation of the signal $E_{\rm vap}$, or of $p(z)$, can be complex as due to the combined effect of the atomic motion and of the surface interaction. Indeed, for nonstationary atoms the coupling between the induced dipole and the incident field is nonlocal [27], since, for a given atomic velocity group (v_z), $p(z, v_z)$ depends on the previous temporal evolution of the atomic dipole. We summarize here some of the effects associated with the atomic motion:

(i) if one neglects the surface interaction, a usual assumption is that the atoms leaving the surface are in the ground state, so that they undergo a transient regime of interaction, while the arriving atoms experience a steady-state interaction with the field. This generates a well-known singularity for atoms of slow normal velocity [27]. In particular, it yields a sub-Doppler component in the SR lineshape, eventually turned into a Doppler-free dispersion-like resonance in a frequency-modulated (FM) scheme [28], when the considered transition is a resonance line starting from a thermally populated ground state;

(ii) when the vW surface interaction is taken into account, both arriving and departing atoms experience a transient regime, but the transient temporal evolution remains considerably different for arriving and departing atoms, and the singularity around the null normal velocity generally survives. A complete analysis, both theoretical [29] and experimental [6–10], of the effect of the surface vW interaction for transitions from the ground state was derived in our previous works. In the framework of linear (FM) spectroscopy under normal incidence, one predicts a simultaneous lineshape distortion, and an apparent frequency shift, governed by the strength C_3 of the atom-surface interaction for the considered transition. These effects are conveniently summarized by a single dimensionless parameter A, defined as:

$$A = 2k^3 C_3/\gamma \qquad (8)$$

(γ is the homogeneous linewidth of the atomic transition). Subsequent extensions of the initial model included the possibility of a residual Doppler broadening (non-normal incidence) [29], finite Doppler width [9], or in related works, of high atomic density effects [30];

(iii) a spatial inhomogeneity in the atomic density ("spatial dispersion" [31,32]) introduces another factor that affects the overall value of $p(z)$. For transitions between excited states, this is expected to be an important effect. The evaluation of $p(z)$ is hence dependent on the mechanism that populates the atoms into the initial state $|i\rangle$ from the ground state (*e.g.* linear or nonlinear optical pumping). In the practical calculation, this adds an extra term in the spatial evolution of $p(z, v_z)$ and implies several extra-steps of integration;

(iv) all of the above description relies on an integration of the contribution of the various velocity groups. This assumes that the effect of the surface interaction is small enough so that the mechanical effects of the interaction potential are negligible. In the conditions of resonant vW interaction, and notably in the repulsive regime, these effects may start to have a realistic influence at typical distances ∼10 nm, that remains however shorter than those explored through the SR technique [5].

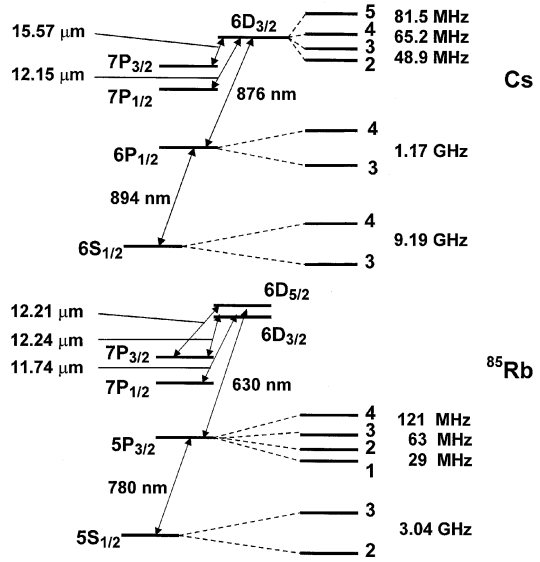

Fig. 5. Scheme of the relevant levels of Cs and Rb, including the hyperfine structure (h.f.s.) when appropriate. For Rb, the indicated h.f.s. applies for ^{85}Rb, the other couplings applying both for ^{85}Rb and ^{87}Rb.

For alkali atoms, whose thermal population lies in the ground state, linear SR spectroscopy cannot be used to probe such levels as Cs(6D), Rb(6D), or Cs(9S), that can be reached only by a two-photon process. The theory of two-photon SR spectroscopy [33] is rather complex and has not included until now the long-range surface interaction. This is why we focused on a situation resembling as close as possible to a resonance line from a thermally populated ground state, enabling us to analyse experimental results with the theory for simple linear SR, whose reliability had been already demonstrated. This purpose was generally achieved by a broadband pumping into the resonant level Cs($6P_{1/2}$) or Rb($5P_{3/2}$) (Fig. 5). The choice of a pumping on the D_1 line for Cs, and on the D_2 line for Rb, has been essentially motivated by the wavelength of the transitions leading to the excited states of interest: frequency tunability across the 921 nm line (for Cs: $6P_{3/2}$–$6D_{3/2}$), or the 620 nm line (for Rb: $5P_{1/2}$–6D) is hardly obtained with c.w. laser diode. When the population of the initial excited state is equivalent to a homogeneous thermal population, the principle of the experimental evaluation of the vW interaction is identical to the one previously established [6–10]. Note that through a single parameter, the theory predicts both the lineshape and its frequency position relatively to the transition for the noninteracting atom. Hence, a revealing test of the quality of the theoretical fitting lies in the agreement between the frequency centre for the atomic resonances, as yielded from the fitting procedure, and an independent determination of this frequency. Also, and as shown in [8], a consistent value of the atom-surface interaction should be deduced independently of the experimental conditions, in spite of the variety of phenomenological lineshapes obtained when varying the pressure conditions (*i.e.* varying the broadening induced by atom-atom collisions). For these reasons,

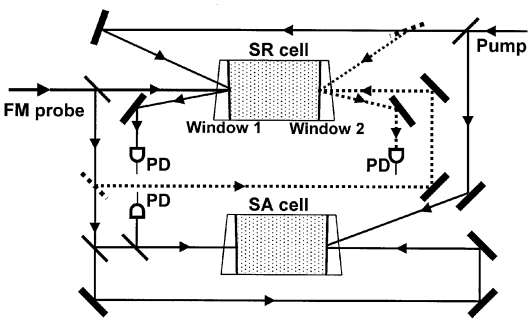

Fig. 6. Principle scheme of the experimental set-up: the removable (dashed) beam splitters, on pump and probe beams, enable simultaneous comparison between 2 windows made of different materials.

the experimental set-up has to provide an auxiliary reference spectrum, free of atom-surface interaction (*e.g.* saturated absorption set-up), and each estimate of a given "excited atom + surface" interaction should result from measurements covering a range of atomic vapour pressure as large as possible.

3.2 Experimental set-up

We describe below the main elements of the experimental set-up employed for probing the $6P_{1/2}$–$6D_{3/2}$ transition of Cs, and we indicate, when appropriate, the changes imposed for probing the Rb transition $5P_{3/2}$–6D, or the Cs transition $6P_{1/2}$–$9S_{1/2}$. A scheme of this set-up is given in Figure 6.

3.2.1 Lasers

An essential element of the experimental set-up is the laser used as the spectroscopic tool for probing the atom-surface interaction through FM SR spectroscopy between excited states. This laser is frequency-modulated, and its frequency stability (jitter and drift) and tunability are essential parameters for the experimental set-up. In all the various experiments that we describe here, this laser is a low-power (<10 mW) semiconductor (s.c.) laser coupled to some other frequency-stabilized external cavity. In the initial steps of the study of the $6P_{1/2}$–$6D_{3/2}$ transition of Cs(876 nm transition), we started from a s.c. chip whose frequency was well-centred relatively to the transition, and we have used the technique of the weak optical feedback from a tunable Fabry-Pérot [34]. In a subsequent step, we have turned to the grating technology, using a commercially designed system. This system has been used to produce the red wavelengths 630.0 nm, 630.1 nm, (for Rb $5P_{3/2}$–$6D_{5/2}$ or $6D_{3/2}$) and 636 nm (for Cs $6P_{1/2}$–$9S_{1/2}$). For the IR emission, the short-term jitter remained well below 1 MHz, and the long-term instabilities (on a few s) induced by the cavity drift were on the order of 2 MHz. For red emission in the 635 nm range, the output power is limited, and the laser has to be operated relatively close

to its threshold. Moreover, our s.c. chip had to be cooled down for emission at 630 nm, while operation at 636 nm (at room temperature) was found to be at the limit of the tunability of the s.c. component. This explains some difficulties observed in the frequency tuning. The FM has been applied through a modulation of the Fabry-Pérot length (most often at ∼52.7 kHz) for the 876 nm laser, or through a modulation (at ∼1.57 kHz) of the grating position in the case of the red lasers. Its peak-to-peak amplitude was chosen in order to remain below the signal resonance width, while maximizing the modulated part in the SR signal (usual *p-p* amplitude in the range 1 to 5 MHz for Cs(6D) experiments, or 5–15 MHz for Rb and Cs(9S) experiments, as due to a lower signal).

The population in the initial resonant state $Cs(6P_{1/2})$ or $Rb(5P_{3/2})$ was produced with another s.c. laser, most often a DBR s.c. laser (free-running jitter <5 MHz, output power up to 50 mW) for the Cs D_1 line (894 nm), or an ordinary s.c. laser (free-running jitter <30 MHz) for the Rb D_2 line (780 nm). In order to generate a nearly thermal population, the pumping mechanism must be large enough to excite all velocity groups. Because SR spectroscopy operates some kind of velocity selection along the normal to the window, off-axis pumping appears preferable; however, the incidence angle is limited due to the geometrical peculiarities of our ovens. Most often, in order to mimic a random distribution of frequency within the Doppler width of the pump transition, we have applied a fast modulation (at ∼200 kHz) of the injected current that induces a large modulation (comparable to the Doppler width ∼200 MHz) of the pump laser frequency. This technique was essentially applied for Rb pumping. For Cs, and as will be discussed in the various tests of the validity of the experimental set-up, the excitation re-distribution inside the resonant $6P_{1/2}$ hyperfine manifold (h.f.s. structure 1.17 GHz), revealed to be a very efficient mechanism (nearly even thermal distribution in the two h.f.s. sublevels) in our pressure range (10–100 mtorr). Because this transfer results from mechanisms such as collisions or radiation trapping that are essentially nonselective with respect to the atomic velocity, even a velocity-selective optical pumping that excites (Cs) atoms in the $6P_{1/2}(F = 4)$ level (respectively $F = 3$) can produce a quasi thermal population on $6P_{1/2}(F = 3)$ (respectively $F = 4$).

3.2.2 Cells and ovens

In all of our experiments, the cells used for SR measurements were sealed vapour cells that were heated-up in an oven whose geometry ensured a slightly higher temperature for the windows than for the alkali metal reservoir (temperature difference ∼10–20 °C, temperature range 100–250 °C). For cells with fused silica windows, the body of the cell was also in fused silica. Cells with sapphire or YAG windows had a sapphire body and were of a special production (in co-operation with the Armenian Institute of Physics). They were either T-shaped, either made of a single sapphire tube, inside which the alkali metal was embedded in a niobium envelope, notably trapping impurities as a getter. Evacuation of these cells, prior to the filling with the alkali metal vapour, normally includes a step at a high temperature (>400 °C) for outgassing [35]. In general, the temperature was measured in two different points with thermocouples probes, supposedly yielding the reservoir temperature and the windows temperature. The vapour pressure (and atomic density) in the cells were extrapolated through classical formulae [36] from the temperature of the alkali reservoir. Note that a gradient of temperature in the cell oven can affect the accuracy of the reservoir temperature. To eliminate this difficulty when comparing the interaction of a given atomic state with various materials, we have notably used cells terminated at one end by a sapphire window — with a nominal *c*-axis normal to the window ($c\perp$) —, and at the other end by a YAG window. For the Cs cell, the orientation of the sapphire *C*-axis was measured to be at 1.8° from the normal to the window. We have also used a Cs cell with a window whose *c*-axis was nearly parallel to the window (actually at ∼10° from the window plane).

3.2.3 Main optical set-up and detection scheme

The incidence angle of the probe beam is most often chosen between 0 and 50 mrad because the expected residual Doppler broadening ($\sim\Gamma_{\mathrm{Dopp}}\theta$) ($\Gamma_{\mathrm{Dopp}} = ku$ being the Doppler shift for an atom flying at the most probable velocity) remains well below the transition linewidth. For the pumping beam, the incidence angle does not exceed 50–100 mrad because of the geometry of the oven. The probe beam is attenuated in order to ensure that the SR signal behaves linearly with the incident intensity. The beam reflected at the window-vapour interface is sent to a low-noise amplified photodiode. The signal is processed through a lock-in amplifier, whose reference channel is synchronous to the FM applied onto the probe beam. For a typical 0.1 mW probe beam, the intensity of the reflected beam falling onto the photodetector is usually on the order of 1 μW, and the typical minimal detectable relative change of reflectivity is usually below 10^{-5}, for an integration time 0.1–1 s. An extra-improvement, by nearly an order of magnitude, leading to a sensitivity close to the shot-noise limit, was finally achieved in the course of the experiments on Rb by applying an additional fast AM on the pump beam. This modulates the population of the initial level of the probed transition ($6P_{1/2}$ for Cs), and it enables a SR signal detection through a cascade of lock-in amplifiers (typically the AM is at 90 kHz, and the FM is hence lowered down into the kHz range).

To provide a spectroscopic reference for a "volume" experiment, an auxiliary experiment has been set that uses fractions of the incident pumping and probe beams. For Cs, a first part of this auxiliary set-up consists of the monitoring of the pumping beam frequency, in order to stabilize the overall atomic density in the (Cs) $6P_{1/2}$ level (as the pump spectrum itself is already broadened, as due to the applied FM). This is usually achieved by a regular linear absorption experiment on a room temperature

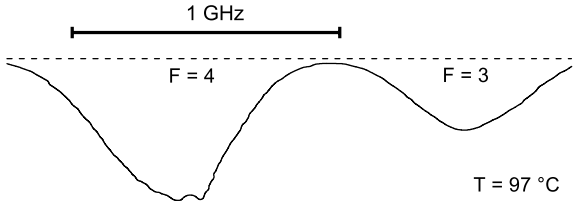

Fig. 7. Linear absorption spectrum on the $6P_{1/2}$–$6D_{3/2}$ transition of Cs (Cs temperature: 97 °C), with the narrow-spectrum pump laser tuned to the $6S_{1/2}(F = 4)$–$6P_{1/2}$ component. One notices on the $6P_{1/2}(F = 4)$–$6D_{3/2}$ component a residual narrow structure related to the hyperfine structure of $6D_{3/2}$, associated to the velocity selectivity in the pumping step; conversely, the $6P_{1/2}(F = 3)$–$6D_{3/2}$ component is observable only because of a collisional redistribution and is intrinsically broad (see text).

cell. A second saturated absorption (SA) set-up is implemented in another Cs cell, for the monitoring of the probe frequency itself. It involves two counterpropagating beams at the probe frequency, in the presence of an additional irradiation at the pumping frequency. It provides the probe frequency reference for the SR spectroscopy experiment that is performed between excited states. Note that because of the hyperfine optical pumping — whose effects are long-lasting in the ground state —, a strong absorption on the pumping transition produces only a relatively low population in the excited states. In order to increase the intermediate state density for the SA experiment, the alkali cell is heated-up. In return, the pump beam is so strongly attenuated in the cell that the SA experiment at the probe frequency is actually performed in a limited region, confined to the vicinity of the window. This was notably the key to perform SA experiments [11], that will be reported elsewhere, characterizing the (atom-atom) collisional behaviour for the $6P_{1/2}$–$6D_{3/2}$ transition of Cs. The pressure broadening was measured to be 1.6 ± 0.4 MHz/mtorr, with an uncertainty mostly related to the temperature measurement, while the pressure shift remained below 0.1 MHz/mtorr, as extrapolated from a Lorentzian fitting of the observed lineshapes.

3.3 Testing the broadband pumping

Because of our purpose to interpret the FM SR spectrum of a transition between excited states on the basis of a SR theory for a transition starting from a thermal ground state, it is particularly important to check if the pumping conditions effectively generates a quasi-thermal population in the $6P_{1/2}$ state for Cs (respectively $5P_{3/2}$ for Rb).

A first test has been provided by the observation of the linear absorption spectrum at the probe frequency in the cell used for the SA reference spectrum. Indeed, the linear absorption spectrum of the probe beam simply reflects the velocity distribution induced in the resonant level (Fig. 7). It easily demonstrates that the chosen pumping conditions provide a broad Gaussian absorption lineshape. In a second step, we have tested directly on the SR spectrum the insensitivity of the SR lineshape to the specific

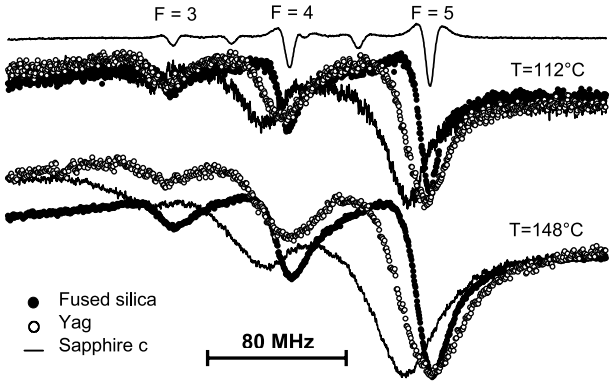

Fig. 8. (FM) SR spectra on the $6P_{1/2}(F = 4)$–$6D_{3/2}$ transition of Cs, recorded for two different temperatures, and various surfaces, along with the SA reference spectrum (upper trace). The amplitudes are normalized, in order to make easier the comparison between the various lineshapes.

parameters (FM broadening of the pump spectrum, residual Doppler broadening, ...) of the pumping process. This appears necessary because the population transfer to the resonant state $6P_{1/2}$, when analysed close to the interface as in a SR measurement, should result also from a transient behaviour, and it may happen that the steady state population is not yet reached. Actually, for all the experiments that we describe below (Sects. 4–6) the tests have been passed successfully.

Also, in the course of these preliminary experiments, it has been observed on Cs (see Sect. 3.2.1) that a velocity-selective pumping (*e.g.* with a narrow laser) on one of the h.f.s. component induces an efficient broadband pumping on the other h.f.s. component, located ∼1 GHz away, in which the initial velocity selection related to the pumping process has disappeared. Note that for Rb, the h.f.s. structure in the $5P_{3/2}$ is smaller than the Doppler width, so that it is not possible to restrict oneself to the broad contribution of atoms that have undergone a hyperfine transfer (hence washing out the initial velocity selection).

4 Interpreting experimental results on Cs($6D_{3/2}$)

4.1 General features of the spectra

Figure 8 shows FM SR spectra as recorded in typical conditions on the $6P_{1/2}(F = 4)$–$6D_{3/2}$ transition of Cs for various cell temperatures (and hence linewidths, as due to pressure broadening). One clearly distinguishes well-resolved Doppler-free structures in all cases, but one notes striking differences according to the considered interface, that can be either fused silica, YAG, or sapphire (with $c\perp$-axis). In particular, one notes that the main differences between YAG and fused silica seem related to the width of the lineshapes, while one notices a systematic red shift of the spectra recorded at the sapphire interface. For the comfort of the eye, the amplitude of the different spectra in Figure 8 has been normalized to their maximum, while

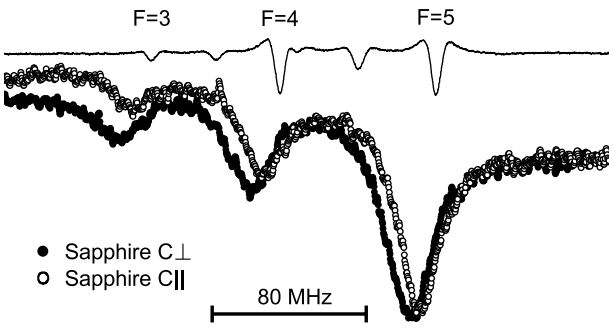

Fig. 9. Comparison between (FM) SR spectra on the $6P_{1/2}(F = 4)$–$6D_{3/2}$ transition of Cs, for sapphire windows with $c\perp$ and $c\|$-axis. The Cs cell temperature is $\sim$105 °C (corresponding to $\sim$0.5 mtorr), and the amplitude of the spectra is normalized. The SA reference spectrum is also indicated.

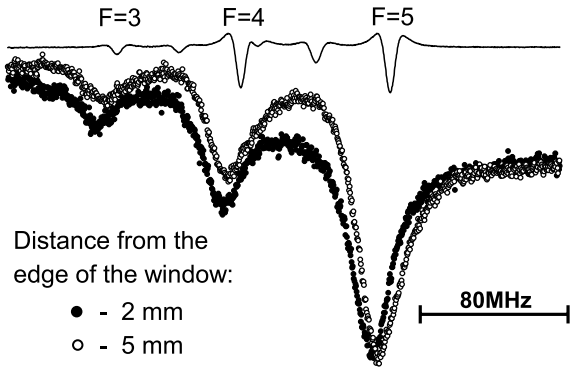

Fig. 10. Comparison between (FM) SR spectra on the $6P_{1/2}(F = 4)$–$6D_{3/2}$ transition of Cs, as recorded for two different positions of the incident beam onto the $c\|$ sapphire window. Varying the stress on the sapphire window, and the related birefringence, appears as a way to tune the resonant behaviour of a sapphire window.

a meaningful comparison should take consideration of the relative signal amplitude. The amplitudes of the SR signal (when compared to the nonresonant reflection) are typically (in the explored temperature range) in a 2.3, 1, 0.6 ratio for fused silica, YAG, and sapphire windows, respectively. Note also that in Figure 8, the vapour temperature should be nearly equal for YAG and sapphire, because the two windows belong to the same cell, while for the fused silica window, the uncertainty in the temperature measurement cannot be neglected. As ascertained below, the large shift, along with other features, observed for the sapphire windows can be intuitively viewed as a signature of a resonant coupling between sapphire polariton mode and the virtual emission of $6D_{3/2}$ of Cs. Note also that for the $6P_{1/2}(F = 3)$–$6D_{3/2}$ manifold, equivalent spectra are obtained, with the h.f.s. components exhibiting more comparable amplitude.

A comparison between two SR spectra recorded respectively on $c\perp$ and $c\|$ sapphire windows, is provided in Figure 9. Clearly, the frequency shift is much weaker for the $c\|$ window. As will be discussed below, this is in agreement with the reduction of the resonant coupling between the polariton mode and the virtual emission of the excited level of Cs. As shown in Figure 10, we have also investigated, for the $c\|$ sapphire window, the influence of the position of the irradiation spot. Close to the regions where the window is glued to the sapphire body of the cell, where stresses and tensions in the window are higher, the spectra are modified, and slightly shifted towards the $c\perp$-window response. It is believed that this relates either with a local change in the c-axis orientation, or more probably, with a stress-induced shift of the surface resonance (*i.e.* it appears as a modification of $\varepsilon_o(\omega)$ and $\varepsilon_e(\omega)$, rather than a geometrical change in the relevant combination of $\varepsilon_o(\omega)$ and $\varepsilon_e(\omega)$).

4.2 Fitting method

Because a quasi-thermal population has been induced in the intermediate level $6P_{1/2}$, the obtained SR lineshapes on the 876 nm line are to be (tentatively) fitted with the previously calculated lineshapes for linear FM SR spectroscopy with vW interaction taken into account. Let us recall that in previous works [29], one has given a detailed numerical evaluation of the FM SR lineshapes for any value of the vW interaction (according to the dimensionless parameter A, see Eq. (8)). The evaluations for this series of lineshapes include a variety of situations, notably perturbative regime of the vW attraction ($0 < A < 1$), strong vW regime ($A > 1$) [29], as well as vW repulsion [5]. The A value governs all the features of the FM spectrum: this includes distortion relatively to the pure Doppler-free dispersive Lorentzian (*i.e.* relatively to the $A = 0$ lineshape), apparent frequency shift relatively to the free-space transition, and signal amplitude (the SR signal being simply proportional to the atomic density, and to the transition probability). It should be recalled that, as a consequence of the spatial averaging intrinsic to the SR method, (see the appendix of [6]) both attractive and repulsive potentials yield an apparent red-shift. However, the lineshapes can be clearly distinguished in most cases, with an exception discussed in Section 4.3.2. In particular, the normalized amplitude (relatively to the vW-free signal, $A = 0$) increases with A ($A > 0$), and decreases with $|A|$ (for $A < 0$). Although the original theoretical lineshapes [29] were calculated in the simple framework of an infinite Doppler width, further improvements in the theoretical lineshape estimates have included the effect of the finite Doppler width (essentially the wings of the FM SR lineshapes) through a first order correction in $\gamma/\Gamma_{\mathrm{Dopp}}$ [9]. Note that the Γ_{Dopp} value is imposed, almost independently of the experimental conditions, while the optical width γ is *a posteriori* deduced in the fitting process (as depending on the experimental conditions). To solve this difficulty, an *a priori* but approximate value of the homogeneous width γ is considered. In the present work, and in

order to increase as much as possible the accuracy of the fitted parameters, the numerical theoretical curves used in the fitting process have been amended to include the effect of the residual Doppler broadening (see [29]) associated with the actual oblique incidence of the probe beam (typical incidence up to 50 mrad). Indeed, some difficulties (see Sect. 4.3.5) have prevented us to perform the experiment too close to the normal incidence. Note that for given experimental data, the major effect of a model including the effect of the residual Doppler broadening, is a slight reduction in the γ value, while A is nearly unaffected (*i.e.* a fraction of the linewidth has to be attributed to the residual Doppler broadening, rather than to the natural width of the atomic transition). Similar effects of apparent broadening are expected from the finite amplitude of the applied FM and the laser jitter (in general assumed to have an infinitely small amplitude).

Experimentally, the neighbouring hyperfine components partially overlap, notably in the wings that are typical of the vW interaction. This profoundly alters the apparent similarity with the lineshape theoretically predicted for an isolated transition. The fitting procedure, based upon a least square method, allows for a theoretical fitting curve that sums over three different hyperfine components. The program is essentially similar to the one previously used in [9]. In spite of numerous free parameters, it achieves convergence efficiently because the hyperfine components are well resolved. For respective trial values A_1, A_2, A_3 of the dimensionless vW interaction strength, the calculation is able to optimise the three respective optical widths γ_1, γ_2, γ_3, the respective amplitudes, as well as the positions of the resonances. It also allows for a residual experimental offset. In such an adjustment, the amplitudes of the three different components can be freely determined, although in the frame of linear FM SR, their relative value is expected to be governed by a factor:

$$(2F+1)(2F'+1)\left\{\begin{array}{ccc} F & 1 & F' \\ 3/2 & 7/2 & 1/2 \end{array}\right\}^2$$

(*i.e.* the 3-2, 3-3, 3-4 components of the $6P_{1/2}(F)$–$6D_{3/2}(F')$ manifold are governed by relative weights 20, 21, 15, and the 4-3, 4-4, and 4-5 components by respective weights 7, 21, 44). Such a flexibility in the amplitudes enables one to take into account possible slight variations of the incident intensity during the laser scan (notably as due to variations in the injected current), as well as residual nonlinear effects, or possible variations affecting the homogeneous linewidth of the components. The extrapolated homogeneous widths γ_1, γ_2, γ_3, can also be determined independently, in spite of the fact that the width, essentially governed by spontaneous or collisional processes, should be identical for each h.f.s. component: this notably permits to compensate for some nonlinearity in the laser frequency scan, that is calibrated thanks to the SA reference spectrum. It is also to allow for residual nonlinearities in the frequency scan that the resonance position of each component of the (well-known) hyperfine structure can be determined independently by the fitting program. In ordinary situations, once an optimal fitting has been found for a given (A_1, A_2, A_3) set of values, it is compared, notably on the basis of the value of the quadratic error, with the other optimal fittings respectively obtained for different sets of values (A'_1, A'_2, A'_3) [37]. This provides a range of acceptable values of the fitting parameters. Naturally, if the set values (A_1, A_2, A_3) is ill-chosen, no satisfactory fit can be obtained. Also, it happens occasionally that some experimental spectrum does not enter inside the family of "fittable" spectra (see Sect. 4.3.5), notably when the linearity of the frequency scan has been altered by severe perturbations. In spite of the numerous free parameters (up to 10 adjustable parameters are to be optimised for a given set (A_1, A_2, A_3)), the fitting procedure remains tractable in most cases, and confidence in the significance of the fitting is ascertained by the agreement with theoretical predictions, not initially included in the fitting method. In particular, the relative amplitudes and the positions of the resonances are in very good agreement with the predictions, the widths of the three resonances are nearly identical, and the set of values (A_1, A_2, A_3) can be most often reduced without losses to a single value of the vW interaction.

In a final stage of improvement of the fitting process, and in order improve the accuracy on the value of the most relevant parameter, *i.e.* $A\gamma$, a reduction in the number of free parameters has been operated, as allowed by the general observations mentioned above. In this approach, an identical value A of the vW interaction is assumed for the three components along with identical widths, while the position of the SR resonances themselves are imposed by the position of the SA resonances (as theoretically expected, with respect to the null pressure shift measured for the $6P_{1/2}$–$6D_{3/2}$ line). Hence, one is left with five adjustable parameters (width, amplitude of each component, and offset) for each fit with a given A value, that can be eventually be reduced to only three by imposing the relative amplitudes of the hyperfine components: in such a case, the discrimination between "good quality fitting" and "bad quality fitting" fits is made even simpler, as long as a nearly ideal fit can be found; this is paid back by the fact that an increasing number of experimental curves may become impossible to be fitted.

4.3 Summary of the results

4.3.1 c⊥ sapphire window

As it has been already described in [5], a consistent series of fits has demonstrated the presence of a strong vW **repulsive** potential at the interface with a $c\perp$ sapphire. The fitting consistency is clearly apparent from two different results. First, one observes, when increasing the Cs density in a significantly large range, a linear increase of the fitting value for γ, while the atom-surface interaction, as determined by the fitting value of the $A\gamma$ product, remains remarkably constant, yielding $C_3 \sim -160 \pm 25$ kHz μm^3 (Fig. 11). This is obtained in

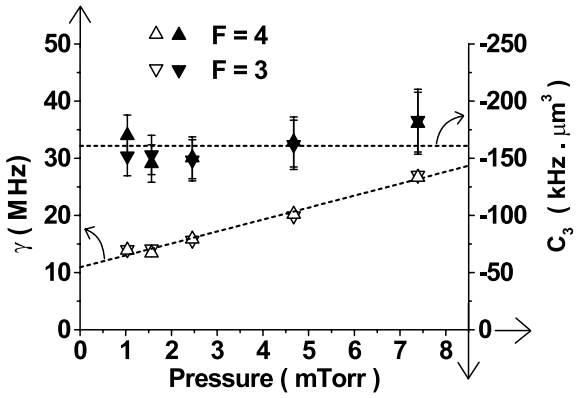

Fig. 11. SR spectroscopy on the $6P_{1/2}$–$6D_{3/2}$ transition of Cs at a sapphire $c\perp$ window: pressure dependence of the fitted values of the optical width and of the vW interaction.

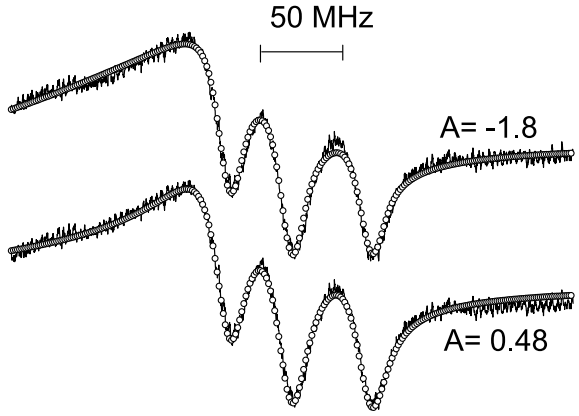

Fig. 12. An example of a FM SR spectrum of Cs($6P_{1/2}(F = 3$)–$6D_{3/2}$) at a YAG interface (125 °C), that can be fitted with a vW attraction (with $C_3 \sim +22.7$ kHz μm^3) or with a vW repulsion with $C_3 \sim -30.5$ kHz μm^3).

spite of the significant changes affecting the spectral lineshapes. Second, for a given atomic density, the two hyperfine manifolds $F = 3 \rightarrow F'$ and $F = 4 \rightarrow F'$, which exhibit notable differences in the overall shape (as related to the different weighting of the various hyperfine component) are actually fitted with extremely similar values (of the A and γ parameters), as expected for an atom-surface interaction that is nearly independent of the considered hyperfine level.

4.3.2 YAG window

As already mentioned, one has observed significant differences between the lineshapes with YAG and with sapphire windows. Initially, the comparison between YAG and sapphire window was implemented because of the expectation that for sapphire, one would be able to demonstrate the possibility of a resonantly enhanced surface interaction (with, in addition, the possibility of getting a repulsive potential), while YAG was supposed to behave nonresonantly, hence leading to the common vW attractive interaction. In some cases, the comparison between the two spectra has been performed in real-time, through a duplicating of the detection set-up, enabling on the same cell (with the two different windows) the simultaneous recording of the two spectra (see Fig. 6). In a first fitting trial, we restricted ourselves to a theoretical model of a vW **attraction**. Fits that look to be acceptable, although not so perfectly fitting as for sapphire, and corresponding to a relatively weak regime of attraction, are obtained if one takes $C_3 \sim +24.5 \pm 5$ kHz μm^3 (Fig. 12). The relative values of the hyperfine components amplitudes are in reasonable agreement with predictions, as well as the consistency of the results when varying the atomic density. However, a surprising point is that for a given cell temperature, the width γ obtained from the fits, is much larger than both the value obtained for the sapphire window (Fig. 13b), and the one deduced from the independent SA measurement. Assuming the possibility of a **repulsive** Cs-YAG vW interaction, consistent fittings have been also obtained, with a typical value of the

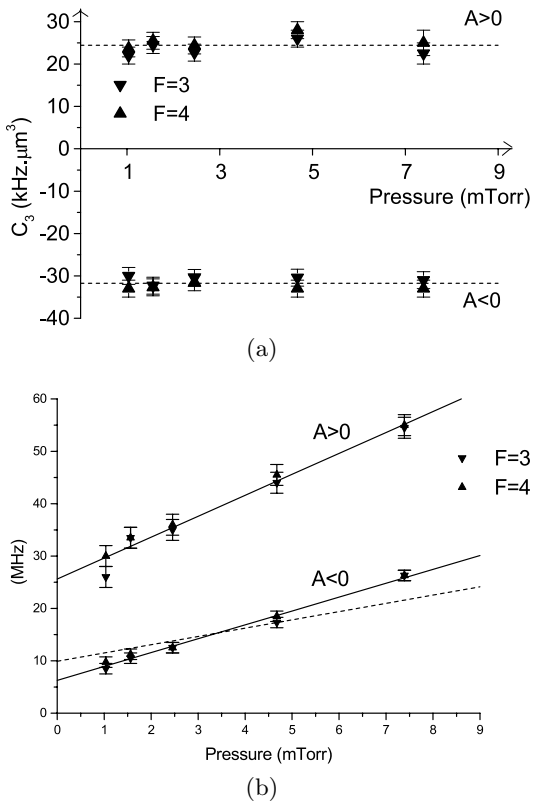

Fig. 13. The ambiguity in the fitting of the SR spectra obtained at a YAG interface on the $6P_{1/2}$–$6D_{3/2}$ transition of Cs: (a) pressure dependence of the fitted values of the vW interaction, assuming either a vW attraction or a vW repulsion; (b) pressure dependence of the fitted values of the optical width, assuming either a vW attraction or a vW repulsion. Both types of fits appear consistent with the phenomenological changes induced by the pressure effects. Only the comparison with an independent measurement (dashed line) performed in a volume experiment, establishes that the vW interaction is actually repulsive (see text).

Table 5. Experimental and theoretical values of C_3 for different atomic transitions, in front of various surfaces. The indicated uncertainties are those found in the frame of the model.

	fused silica $Cs(6P_{1/2}–6D_{3/2})$	YAG $Cs(6P_{1/2}–6D_{3/2})$	sapphire ($c\perp$) $Cs(6P_{1/2}–6D_{3/2})$	fused silica $Cs(6P_{1/2}–9S_{1/2})$	sapphire ($c\perp$) $Cs(6P_{1/2}–9S_{1/2})$
C_3 (kHz μm^3) with fit	11 ± 2	-32 ± 5	-160 ± 25	130 ± 15	100 ± 10
C_3 (kHz μm^3) with tables	9.4	-18.3	-98.6	93	52

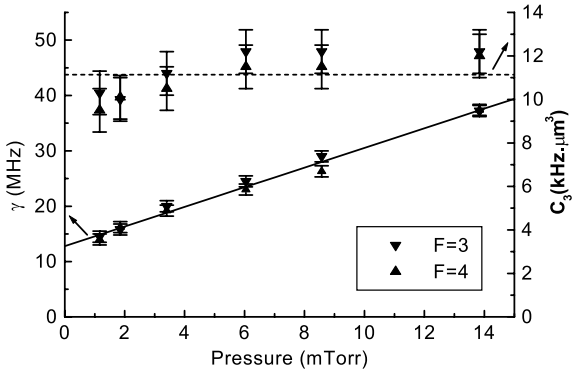

Fig. 14. SR spectroscopy on the $6P_{1/2}$–$6D_{3/2}$ transition of Cs at a fused silica interface: pressure dependence of the fitted values of the optical width and of the vW interaction.

vW repulsion, on the order of $C_3 = -32 \pm 5$ kHz μm^3, as illustrated in Figure 13a. The main difference with the fitting for a vW attraction is that the pressure broadening behaviour becomes in good agreement with the values measured both on the sapphire window and in the volume experiment. This ambiguity between the lineshapes for vW repulsion and vW attraction, finally resolved only thanks to the overall measurement of the pressure broadening, originates in the large similarity in the lineshapes in the typical ranges $0.3 \leq A \leq 2$ and $-2 \leq A \leq -0.3$, *i.e.* when the most apparent effect of the vW perturbation (whatever its sign may be) is to induce an apparent redshift (see [6] and the discussion in Appendix). Returning to the theoretical expectations, one finally sees that the experimental results are thus in good agreement with the moderate vW repulsion that has been predicted for YAG (see Sect. 3).

4.3.3 Fused silica window

The experimental FM SR lineshapes for a Cs cell terminated by a glass window (fused silica) have been also successfully fitted with the SR lineshapes that include the effect of a vW potential. The fitting consistently establishes, without further ambiguity, that the vW interaction is weakly attractive. Results of the fitting are shown in Figure 14, leading to $C_3 = 11 \pm 2$ kHz μm^3, in an excellent agreement with the theoretical prediction (Tabs. 1 and 5). Note that, due to a weak dispersive resonance for a fused silica surface in the 12 μm range, an accurate prediction depends strongly on the exact parameters of the fused silica window (temperature, etc.) [18].

4.3.4 Sapphire window (c||)

One has observed notable experimental differences between SR spectra at the interface with a sapphire window according to the c-axis orientation, either perpendicular to the window ($c\perp$), or parallel to the window ($c\|$). From a theoretical point of view, the c-axis, when not perpendicular to the window, induces a break of the cylindrical symmetry of the problem, and a complete theoretical approach cannot be limited to the $(D^2 + D_z^2)/z^3$ effective Hamiltonian. One expects a degeneracy lifting between the various atomic states (according to m_J) [4,38]. This should induce a dependence of SR spectra on the incident probe polarization, and the corresponding excitation of a specific h.f.s. component. Actually, we have not found a significant sensitivity to the polarization, most probably because with a ($c\|$) window, the potential gets weaker, due to the polariton frequency shift [4].

In the absence of a clear signature of a symmetry break, it has appeared reasonable to attempt a fitting of the experimental lineshapes with the scalar theoretical model described in Section 4. Such tentative fits have demonstrated that the strong resonant repulsion evidenced with the $c\perp$ sapphire window disappeared. However, at the point of deciding which sets of fitting parameters are acceptable, and which one should be rejected, the situation is even more intricate than the one discussed in the case of YAG (Sect. 4.3.2) when attractive or repulsive interaction induces comparable lineshapes features. Also, the agreement between the tentative fits, and the experiments remains rather poor (in the wings, in the linewidth, etc.). Indeed, the shift of the polariton resonance (relatively to the resonance of a $c(\perp)$ window) implies a severe decrease of the contribution of the 12.15 μm line, which is no longer the dominant one. As a consequence the overall prediction becomes inaccurate (*e.g.* $-25 \leq C_3 \leq 25$ kHz μm^3). As will be reported elsewhere [39], a satisfactory agreement needs one to include in the physical model the dissipative effect of the real energy transfer, that is also z^{-3} space-dependent (see [40] and the experimental observation in [32]), in addition to the vW energy shift originating in the virtual emission.

4.3.5 A remark

Before closing this section devoted to the fine agreement obtained between the experiment and the fitting model, we should mention that we observed that the lineshape is modified for an irradiation very close to the normal incidence, with the appearance of a narrow structure [11].

This structure can never be fitted within the model, it is more or less dispersion-like, and has an apparent width on the order of the natural width. Remarkably, this structure can be observed for various types of windows, independently of the strength of the vW interaction, and it is precisely located on linecenter (as estimated for a free atom, as it would be the case if originating from a signature of atoms relatively far away from the wall). Although we have not been able to build-up a satisfactory model, we believe that this signal may be related with an inhomogeneous spatial distribution of atoms: in particular, when the transient evolution of the pumping is considered, the density of departing atoms is expected to be inhomogeneous on distances on the order of the wavelength. This effect, most probably hindered in the transmission experiments, remains however marginal enough to disappear with a relatively small amount of broadening (*e.g.*: FM amplitude, residual Doppler broadening, pressure broadening...). It is also independent of the pumping conditions (Sect. 3.3).

5 Experimental results on Rb(6D)

5.1 Main differences with the 6P–6D transition of Cs

The essential interest of studying the 5P–6D transition of Rb, is that the 6D level couples to Rb(7P) at wavelengths that fall in near coincidence with the Cs $6D_{3/2} \rightarrow 7P_{1/2}$ coupling, whose dramatic effects in the vicinity of a sapphire or of YAG surface have been seen in the previous section. In the principle, exploring the resonant coupling at wavelength neighbouring the one of the Cs 6D line should provide some kind of high resolution spectroscopy of the surface polariton resonance of sapphire and YAG. Moreover, while the Cs $6D_{5/2} \rightarrow 7P_{3/2}$ coupling is simply non resonant, but that no comparison experiment could be performed because of the difficulty to reach $Cs(6D_{5/2})$ — an uncommon source at 917 nm would be required following a pumping tuned to the D_2 resonance line —, in the case of Rb, the fine structure levels $6D_{3/2}$ and $6D_{5/2}$ are expected to exhibit a resonant behaviour with sapphire or YAG surface. The 6D–7P coupling falls indeed respectively at 12.21 μm and 11.74 μm (and 12.24 μm). For such a comparison, the pumping is necessarily on the D_2 line (780 nm). This is actually more favourable than a D_1 pumping, as the excitation line to 6D falls then in the 630 nm range (630.0 nm and 630.1 nm), where some diode lasers operate, while the 620 nm range required with a D_1 pumping cannot presently be reached with a diode laser.

Unfortunately, it has appeared that several differences between the Rb experiment and the Cs experiment, that we list below, have imposed severe limits on the Rb studies:

(i) in spite of an apparent similar labelling, Rb(6D) is a more excited level than Cs(6D), both energetically (3.6 eV instead of 2.8 eV), and in the number of quantized excitation: it is more resembling to a Rydberg level, has a longer natural lifetime (295 ns *vs.* 70 ns), so that the transition probability 5P–6D of Rb is approximately one order of magnitude smaller than the one of 6P–6D of Cs. In a *linear* technique such as SR spectroscopy, this limits practically the sensitivity: the only possible compensation is found in increasing the atomic density. In return, the narrow spectral features, from which the vW interaction can be characterized, undergo a considerable pressure broadening;

(ii) as expected for a higher-lying state, the hyperfine structure of Rb(6D) is much narrower (in the range 1–8 MHz, depending on the considered manifold) [41] than in the well-resolved one of Cs(6D). Even in the low-pressure SA reference spectra, the h.f.s. of Rb(6D) cannot be resolved for most of the transitions, and the SR spectra appear simply broadened by the unresolved h.f.s.;

(iii) natural Rb is a mixture of two isotopes. For the first resonance line (D_1 or D_2), the relevant isotope shifts are rather large, so that all transitions are easily discriminated. However, radiation redistribution in the resonant level can transfer excitation from one isotope to the other one. Because the two isotopes have close 5P–6D lines, the wing analysis, so important in the fit analysis for a correct determination of the vW interaction, can be made more difficult by these residual contributions.

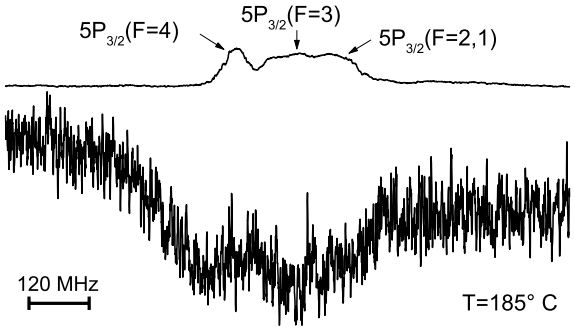

Fig. 15. (FM) SR spectrum as recorded on the weak $5P_{3/2}$–$6D_{3/2}$ transition of Rb at fused silica interface. Note the high pressure broadening of Rb.

5.2 SR spectra: comparison between different windows

In spite of all our attempts, notably including focusing of the pump beam — at the risk of saturation effects — to increase the atomic density in the excited state, the SR spectrum on the weak $5P_{3/2}$–$6D_{3/2}$ transition has been observable only in pressure conditions that imply a broadening hardly compatible with the detection of surface interaction effects. This is illustrated in Figure 15: the signal remains small while the pressure broadening tends to induce an overlap between the hyperfine components of the initial states of the transition.

The transition $5P_{3/2}$–$6D_{5/2}$ has revealed to be more favourable, and we succeeded in performing significant comparison between SR spectra at the interface with different types of windows. At the interface with a fused silica

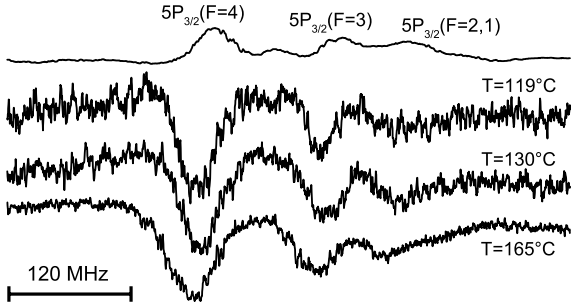

Fig. 16. (FM) SR spectrum as recorded at fused silica interface on the $5P_{3/2}$–$6D_{5/2}$ transition of Rb.

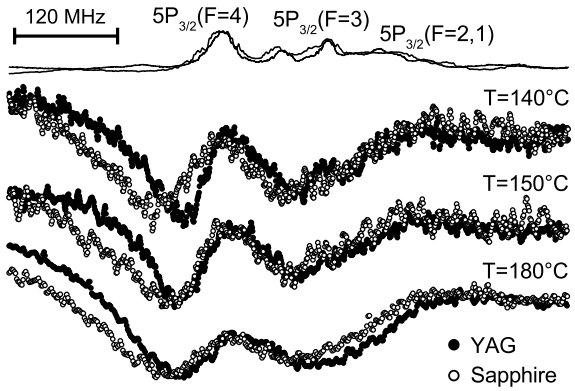

Fig. 17. Comparison between (FM) SR spectrum as recorded at YAG (dot line) and sapphire ($c\perp$) interfaces on the $5P_{3/2}$–$6D_{5/2}$ transition of Rb. Because all the available laser power is needed in a single experiment, the comparison between YAG and sapphire has not been performed with simultaneous recordings. The occasional frequency drifts are visible from the SA reference where two successive frequency scans are presented.

window, the SR spectrum resonances, although as broad as 50 MHz, do not exhibit a significant frequency shift. The SR peak remains within 20 MHz from the position of the SA resonance. The SR lineshape, as seen in Figure 16, is always asymmetric, and evolves smoothly with the broadening induced by increasing temperature and densities. In spite of the complexity brought by the successive hyperfine components, one may recognize the typical distortion induced by a relatively weak vW (attractive) interaction (as expected for a non resonant atom-surface interaction).

This contrasts with the situation observed with the cell terminated by sapphire ($c\perp$) and YAG windows. Between the spectra recorded at the same temperature with these two windows, one notices considerable differences, as seen from Figure 17. With the sapphire window, one notes a considerable red frequency shift relatively to the SR spectrum on the YAG window, and to the SA resonance. This red shift at the sapphire interface is observed with a comparable line broadening. The SR spectrum at a YAG interface also shows a red-shift relatively to the SA resonance peak, while the SR wing are considerably broadened relatively to the one of a SR spectrum at a fused silica interface.

These behaviours, notwithstanding a smaller overall amplitude, with respect to the fused silica window are typical of a repulsive vW interaction, and can be seen as an indication for a resonant behaviour in the atom-surface interaction induced by the coupling between the Rb ($6D_{5/2}$) emission at 12.21 μm, and the surface resonances of sapphire and of YAG.

However, the pressure broadening has remained very large for all spectra exhibiting a reasonable signal amplitude, while the frequency reference itself is relatively noisy. This is why we have not attempted to fit the recorded SR spectra.

6 Cs(9S) and the SiO_2 resonance in the 8 μm range

6.1 Differences with the other experiments

The previously analysed experiments were motivated by some specific resonance of sapphire, that could be extended to YAG, while the fused silica window was the typical example of a nonresonant material. Here, it appears in Table 4, that, with regards to its surface vW interaction, the high lying state 9S of Cs is mainly sensitive to the couplings at 12.96 μm and 13.76 μm, along with those at 8.3 μm and 8.9 μm. However, the couplings in the 13 μm region are not affected by the above demonstrated sapphire resonance, because they simply correspond to a virtual absorption; conversely, the couplings in the 8 μm range are associated to a virtual emission, susceptible of a resonant exchange with the surface mode. Specifically, for the fused silica, there is simultaneously a large resonant enhancement of the 8.9 μm contribution, and a negative resonant behaviour for the companion coupling at 8.3 μm. For the sapphire, the coupling in the 8–9 μm region reduces the vW attraction, because of the far wing of the 12 μm resonance. It is hence one of the situation where the interaction on the fused silica window should be an attraction stronger than the one of sapphire, mainly because of the resonant contribution of the fused silica. With the exception of strong resonances, this situation can appear to be unusual as it is at the opposite of the ratio of the index of refraction (higher for sapphire than for fused silica at the wavelength of observation).

The experiments, performed by SR spectroscopy on the $6P_{1/2}$–$9S_{1/2}$ line after a D_1 line pumping, benefit on the one hand of the well-resolved h.f.s. of the $9S_{1/2}$ level, whose splitting is as large as 440 MHz, so that even at high Cs pressure, there is never any overlap between the various components, while on the other hand, the transition probability (and accordingly the SR signal) is weaker by an order magnitude than on the $6P_{1/2}$–$6D_{3/2}$ line; additionally, the frequency tuning of the laser can reveal to be difficult in this frequency range. This is why we have only realized a limited set of experiments, not exploring

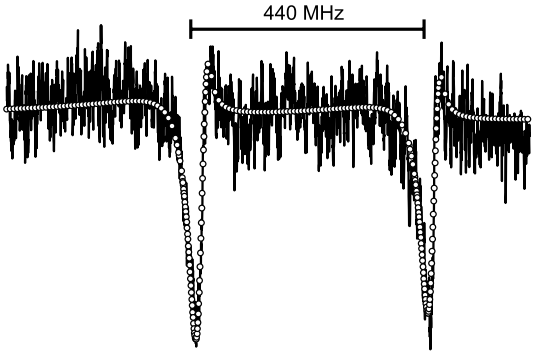

Fig. 18. (FM) SR spectrum on the $6P_{1/2}$–$9S_{1/2}$ transition of Cs at sapphire window ($c\perp$). The fit is also indicated (open circles).

much the variations of the SR behaviour with the Cs density, nor attempting to study systematically the possible pressure-shift affecting the volume (SA) reference.

6.2 Experimental results and interpretation

The experiments have been limited to the comparison of a sapphire window (c-axis perpendicular to the window) and of a fused quartz window. There was no effective attempt of including the high density effects: conversely, spectra were recorded several times in similar nominal conditions, in order to minimize fluctuations in the frequency scan. To eliminate as much as possible the need of an estimate of the frequency shifts induced by pressure for the volume resonance, the SR lineshapes were recorded in the conditions of a low atomic density (typically 130–140 °C of Cs, *i.e.* $\approx 10^{14}$ at/cm^3). However, this was obtained at the expense of the signal-to-noise ratio, whose optimisation hence depends on the adjustment of the FM amplitude. This is why, for this set of experiments, the FM amplitude is much larger than for the $6P_{1/2}$–$6D_{3/2}$ and can reach an appreciable fraction of the linewidth, implying a residual FM broadening that can easily remain unnoticed at the time of the experiment, as due to the low signal to-noise ratio.

A typical SR spectrum is presented in Figure 18, as recorded at an interface with a sapphire window, along with the best corresponding fitting. Here again, and in spite of the possible effects of spatial dispersion always associated to a first pumping step, we obtain an excellent agreement between the experimental SR lineshape, and the chosen calculated lineshape. As an evidence of the good quality of the fitting, it should be noted that, here again, the two h.f.s. components are fitted with the same width and vW interaction although they are perfectly resolved. Relatively to the fitting method described in the Section 4.2, the presented fitting has been improved by taking into account the effect of this modulation frequency. A smoothing method is indeed applied to the ideal theoretical curve. As a rule, this implies a slightly reduced value of the extrapolated value of γ and can tend simultaneously to modify the optimal value of the vW parameter A. One also notes that the central position of the resonance, as deduced from the SR lineshape, is automatically adjusted from the fitting programme, and is slightly redshifted (by an amount 4–5 MHz) relatively to the low Cs-density SA reference. This appears very compatible with a small pressure-induced shift: indeed an identical shift is obtained for a fitting of the SR spectrum at a fused silica interface at comparable Cs densities.

From the systematic analysis of the data, and of the corresponding fits, we conclude that the C_3 values, estimated experimentally to be: (100 ± 10) kHz μm^3 for sapphire ($c\perp$), and (130 ± 15) kHz μm^3 for fused silica, are larger than the predicted values by a factor not exceeding 2, and that the fused silica interface is responsible for a stronger interaction than the sapphire. Although the cells are not identical, one may estimate that most of the systematic errors that could affect the C_3 value should be identical in the two SR experiments, confirming again experimentally that the fused silica exerts on the Cs $9S_{1/2}$ level an enhanced attraction due to a pole in the 8–9 μm range.

7 Conclusion

The above extended experimental study completes the first evidence of a resonant vW atom- surface interaction that is turned into a repulsion. Along with the general interest for the control of atom-surface interaction, it clearly shows that this repulsion, that may look to be exotic in its requirement of a coincidence between the atom and the surface mode resonances, is actually more common than expected at first sight. In particular, for high-lying atomic states, the stronger couplings are in the infrared range, and naturally fall in a range where the dispersive properties of dielectric windows can induce strong resonances.

As mentioned in Section 2, one should expect large uncertainties concerning the resonant features of the surface polariton modes, notably because of a possible dependence on the sample, and a lack of data obtained at the adequate surface temperature, moreover in a wavelength range that makes the "window" strongly opaque. In addition, in some cases, the C_3 predictions may depend on the surface response rather far away from the resonance center (this is the case for the 9 μm behavior of sapphire for Cs(9S)), or on a combination of various resonant behaviors (*e.g.* the repulsive contribution at 8.3 μm for Cs($9S_{1/2}$) in front of fused silica, as opposed to the enhanced attractive contribution of the 8.9 μm transition). Table 5, that summarizes the results of the comparison between the predicted C_3 values (for a given *transition*, *i.e.* taking into account the minor effect of the C_3 value of the lower state), and the experimental findings, shows an agreement satisfactory up to a level on the order of 50%. Such a good agreement is even remarkable in view of the various pitfalls that could affect it: the model used for the theory is somehow crude in its neglect of the spatial dispersion of the pumped atoms (notably for departing atoms). It also neglects the spatial dependence $\gamma(z)$ of the relaxation coefficient γ induced for all emission transitions

by the process of fluorescence in an evanescent mode [42], and, for the resonant coupling, by the near-field z^{-3} real transfer [32]. It is indeed only for $c\|$ sapphire that the latter effect must be introduced, in a more refined fitting process that will be presented elsewhere [39]. It should be added that in the present study, when the signal-to-noise ratio and the frequency resolution allow one to attempt a fitting method, the fitting model based upon an initial thermal population has revealed to be very efficient: this shows once again how powerful is the FM SR technique, with its intrinsic velocity selection. Only in some cases the consideration of the broadening induced by the finite amplitude of the applied FM has improved, to a limited extent, the quality of the fittings.

A further extension of this work, which actually represents, to our knowledge, the sole observation of the very fundamental process of long range energy exchange between an excited atom and a real surface, should notably include the cavity QED correction for non-zero temperature [43]. Indeed, the strong 12 μm emission coupling in our experiment is only $\sim$3 times more energetic than the average quantum of thermal excitation, so that the reverse process (resonant coupling due to a virtual atomic absorption) may start to be observable, or turn to be dominant for higher-lying levels, as is the Cs(8P) level, that we are presently exploring [44]. At last, for these thermal effects, a foreseen difficulty lies in the fact that the surface resonances themselves are extracted from phenomenological values of the optical parameters of the dielectric material: these dispersive properties of the windows are usually temperature-dependent, and this dependence can partly be traced back to thermal statistics effects, like multiphonon absorption [45].

One of us (H.F.) would like to acknowledge the support of a grant of the French Government, and the permanent support of the IFFI, Montevideo. Work also partly supported by the French-Uruguayan cooperation (ECOS-Sud project U00-E03) and completed in partial requirement of the FASTNet project (European network HPRN-CT-2002-00304).

References

1. J.E. Lennard-Jones, Trans. Faraday. Soc. **28**, 334 (1932)
2. J.M. Wylie, J.E. Sipe, Phys. Rev. A **32**, 2030 (1985); **30**, 1185 (1984) and references therein
3. M. Fichet, F. Schuller, D. Bloch, M. Ducloy, Phys. Rev. A **51**, 1553 (1995)
4. M.P. Gorza, S. Saltiel, H. Failache, M. Ducloy, Eur. Phys. J. D **15**, 113 (2001)
5. H. Failache, S. Saltiel, M. Fichet, D. Bloch, M. Ducloy, Phys. Rev. Lett. **83**, 5467 (1999)
6. M. Chevrollier, M. Fichet, M. Oria, G. Rahmat, D. Bloch, M. Ducloy, J. Phys. II France **2**, 631 (1992)
7. M. Oria, M. Chevrollier, D. Bloch, M. Fichet, M. Ducloy, Europhys. Lett. **14**, 527 (1991)
8. M. Chevrollier, D. Bloch, G. Rahmat, M. Ducloy, Opt. Lett. **16**, 1879 (1991)
9. N. Papageorgiou, M. Fichet, V.A. Sautenkov, D. Bloch, M. Ducloy, Laser Phys. **4**, 392 (1994)
10. M. Gorris-Neveux, P. Monnot, M. Fichet, M. Ducloy, R. Barbé, J.C. Keller, Opt. Commun. **134**, 85 (1997)
11. H. Failache, Ph.D. thesis, University of Paris-13, 1999
12. A.S. Barker, Phys. Rev. **132**, 1474 (1963)
13. The interaction between an atom and a perfectly reflecting surface has been studied for a very long-time. Review articles, on both theory and experiment, can be found in S. Haroche, in *Fundamental Systems in Quantum Optics*, edited by J. Dalibard, J.M. Raimond, J. Zinn-Justin (North Holland, Amsterdam, 1992), p. 767 and in reference [14]
14. E.A. Hinds, Adv. At. Mol. Opt. Phys. Supp. **2**, 1 (1994), and references therein; see also: V. Sandoghdar, C.I. Sukenik, S. Haroche, E.A. Hinds, Phys. Rev. A **53**, 1919 (1996)
15. H.B.G. Casimir, D. Polder, Phys. Rev. **73**, 360 (1948)
16. D. Meschede, W. Jhe, E.A. Hinds, Phys. Rev. A **41**, 1587 (1990); J. Dalibard, J. Dupont-Roc, C. Cohen Tannoudji, J. Phys. France **43**, 1617 (1982)
17. C. Mavroyannis, Mol. Phys. **6**, 593 (1963)
18. S. Saltiel *et al.* (to be published)
19. A.K. Harman, S. Ninomiya, S. Adachi, J. Appl. Phys. **76**, 8032 (1994)
20. H.R. Philipp, in *Handbook of optical constants in solids I*, edited by E.D. Palik, 2nd edn. (Academic Press, 1988), p. 749
21. G.A. Gledhill, P.M. Nikolic, A. Hamilton, S. Stojilkovic, V. Blagojevic, P. Mihajlovic, S. Djuric, Phys. Stat. Sol. (b) **163**, K123 (1991)
22. Our C_3 value does not include the polarization of the core, see A. Derevianko, W.R. Johnson, M.S. Safronova, J.F. Babb, Phys. Rev. Lett. **82**, 3589 (1999)
23. O.S. Heavens, J. Opt. Soc. Am. **51**, 1058 (1961)
24. A. Lindgard, S.E. Nielsen, At. Data Nucl. Data Tables **19**, 612 (1977)
25. In Tables 1–3, it is assumed that all hyperfine sublevels undergo the same interaction with the surface. It is a good approximation when the preparation of state is isotropic
26. A. Landragin, J.-Y. Courtois, G. Labeyrie, N. Vansteenkiste, C.I. Westbrook, A. Aspect, Phys. Rev. Lett. **77**, 1464 (1996); R.E. Grisenti, W. Schöllkopf, J.P. Toennies, G.C. Hegerfeldt, T. Köhler, Phys. Rev. Lett. **83**, 1755 (1999); M. Boustimi, B. Viaris de Lesegno, J. Baudon, J. Robert, M. Ducloy, Phys. Rev. Lett. **86**, 2766 (2001)
27. M.F.H. Schuurmans, J. Phys. France **36**, 469 (1976); G. Nienhuis, F. Schuller, M. Ducloy, Phys Rev. A **38**, 5197 (1988)
28. A.M. Akul'shin, V.L. Velichanskii, A.S. Zibrov, V.V. Nikitin, V.A. Sautenkov, E.K. Yurkin, N.V. Senkov, JETP Lett. **36**, 303 (1982)
29. M. Ducloy, M. Fichet, J. Phys. II France **1**, 1429 (1991)
30. Ping Wang, A. Gallagher, J. Cooper, Phys Rev. A **56**, 1598 (1997), and references therein
31. H. van Kampen, V.A. Sautenkov, E.R. Eliel, J.P. Woerdman, Phys Rev. A **58**, 4473 (1998)
32. H. Failache, S. Saltiel, A. Fischer, D. Bloch, M. Ducloy, Phys. Rev. Lett. **88**, 243603 (2002)
33. O.A. Rabi *et al.*, Europhys. Lett. **25** 579 (1994); A. Amy-Klein *et al.*, Phys. Rev. A **52**, 3101 (1995); M. Gorris-Neveux *et al.*, Phys. Rev. A **54**, 1 (1996); F. Schuller *et al.*, Phys. Rev. A **47**, 519 (1993)

34. B. Dahmani, L. Hollberg, R. Drullinger, Opt. Lett. **12**, 876 (1987)
35. In some cases, it happened that we observed a reversible formation of an opaque layer on the surface in the course of an intense resonant irradiation to the highly excited states 6D of Cs or Rb [11]. We have attributed [R. Vetter, private communication] these effects, that make the SR spectra unreliable, to a residual gas in the vapour (most probably hydrogen)
36. J.B. Taylor, I. Langmuir, Phys. Rev. **51**, 753 (1937)
37. Because the vW (FM) SR lineshapes – governed by the dimensionless A parameter – are only numerically calculated for a discrete set of A values, but not evaluated analytically, the optimisation method by the least square fit cannot be applied on the A parameter
38. In the principle, the polarization of the pumping irradiation may have its own influence, related to state preparation, in situations when the efficiency of the resonant pumping depends on the considered sublevels, but the collisional redistribution mechanisms that are involved in the pumping process should naturally make this effect negligible. For the case of vW shift dependent on magnetic field, see N. Papageorgiou, Ph.D. dissertation, Université Paris-13, December 1994; N. Papageorgiou, D. Bloch, M. Ducloy, B. Gross, F. Baur, A. Weis, Ann. Phys. Fr. **20**, 611 (1995)
39. M. Fichet *et al.*, to be published and abstract EF3T of EQEC2003-Munich. In this work, the effects of the dissipative coupling, that goes along with resonant atom-surface coupling, will be also introduced for sapphire ($c\perp$) and YAG
40. M. Fichet, F. Schuller, D. Bloch, M. Ducloy, Ann. Phys. Fr. **20**, 649 (1995)
41. E. Arimondo, M. Inguscio, P. Violino, Rev. Mod. Phys. **49**, 31 (1977)
42. W. Lukosz, Opt. Commun. **20**, 195 (1977)
43. M.P. Gorza *et al.*, to be published and abstract EH5M of EQEC2003-Munich
44. I. Hamdi *et al.*, to be published and abstract EF2M of EQEC2003-Munich
45. M.E. Thomas, R.I. Joseph, W.J. Tropf, Appl. Opt. **27**, 239 (1988)